*minerals*

MDPI

*Article*

# Lead–Antimony Sulfosalts from Tuscany (Italy). XXIV. Crystal Structure of Thallium-Bearing Chovanite, $TlPb_{26}(Sb,As)_{31}S_{72}O$, from the Monte Arsiccio Mine, Apuan Alps

**Cristian Biagioni [1,*], Yves Moëlo [2], Natale Perchiazzi [1], Nicola Demitri [3] and Giovanni Orazio Lepore [4]**

1 Dipartimento di Scienze della Terra, Università di Pisa, Via Santa Maria 53, I-56126 Pisa, Italy; natale.perchiazzi@unipi.it
2 Institut des Matériaux Jean Rouxel, UMR 6502, CNRS, Université de Nantes, 2, rue de la Houssinière, F-44322 Nantes CEDEX 3, France; Yves.Moelo@cnrs-imn.fr
3 Elettra–Sincrotrone Trieste S.C.p.A., S.S. 14 km 163,5 in Area Science Park, Basovizza, I-34149 Trieste, Italy; nicola.demitri@elettra.eu
4 CNR-IOM-OGG, 71 Avenue des Martyrs, F-38043 Grenoble, France; lepore@esrf.fr
* Correspondence: cristian.biagioni@unipi.it; Tel.: +39-050-221-5789

Received: 22 October 2018; Accepted: 16 November 2018; Published: 18 November 2018


**Abstract:** A thallium-bearing variety of the lead–antimony oxysulfosalt chovanite from the Monte Arsiccio mine (Apuan Alps, Tuscany, Italy) has been reexamined. It occurs as thin, ribbon-like crystals, black in color, up to 5 mm in length in vugs of dolomite ± baryte ± quartz veins embedded in the metadolostone of the Sant'Olga level. Associated minerals are rouxelite, robinsonite, sphalerite, valentinite, baryte, dolomite, quartz, and Ba-rich K-feldspar. Chemical analysis pointed to contents of Tl up to 0.86 apfu, corresponding to the ideal chemical formula $TlPb_{26}(Sb,As)_{31}S_{72}O$. The structural role of thallium has been investigated using single-crystal X-ray diffraction using synchrotron radiation ($\lambda$ = 0.59040 Å). Thallium-rich chovanite is monoclinic, space group $P2_1/c$, with unit-cell parameters $a$ = 34.280(3), $b$ = 8.2430(7), $c$ = 48.457(4) Å, $\beta$ = 106.290(4)°, and $V$ = 13143(2) Å$^3$. The crystal structure was refined to a final $R_1$ = 0.083 for 12,052 reflections with $F_o > 4\sigma(F_o)$ and 1210 refined parameters. The general features of thallium-rich chovanite agree with those of chovanite. Thallium is present as $Tl^+$; it is disordered among two mixed (Pb/Tl) positions, with a Tl/Pb atomic ratio below 1, that precludes this compound to be a new species.

**Keywords:** chovanite; sulfosalt; thallium; lead; antimony; oxygen; crystal structure; Monte Arsiccio mine; Apuan Alps; Italy

## 1. Introduction

Chovanite is one of the few lead–antimony oxysulfosalts found in nature and it has been reported from very few localities worldwide. Chovanite was first described from three Sb deposits in the Low Tatra Mountains, Slovakia [1] and, later, was found in two small neighboring pyrite ± baryte ± iron oxide ore deposits from the Southern Apuan Alps, i.e., the Pollone and Monte Arsiccio mines [2]. These latter findings allowed a better description of the crystal-chemistry of chovanite, whose ideal formula can be written as $Pb_{28}Sb_{30}S_{72}O$. In addition, the Italian occurrences showed interesting chemical features, such as the high As content (up to 5.20 atoms per formula unit, apfu) in the sample from the Pollone mine or the significant Tl content (up to 0.86 apfu) in the specimen from the Monte Arsiccio mine. Whereas the crystal structure of the former specimen was solved and refined, owing to

the relatively high quality of the available material, the sample from Monte Arsiccio was represented by ribbon-like fibers, sometimes bent, that gave poor diffraction patterns, allowing the refinement of the 4 Å structure converging to an $R_1$ value of 0.235% [2]. However, the high thallium content prompted the search for crystals suitable for single-crystal X-ray diffraction studies, in order to describe the thallium distribution in this complex sulfosalt. This could correspond either to a new mineral species (if thallium is preferentially partitioned at one site) or to a thallium-bearing variety (if this element is disordered among several positions, without being dominant in at least one of them). Finally, a very small individual was found having a relatively better diffraction pattern and allowing a single-crystal X-ray diffraction investigation. Owing to the small size of this crystal, synchrotron radiation was used for the intensity data collection.

The crystal structure of this thallium-bearing chovanite is described in this paper.

## 2. Sample Description

Thallium-bearing chovanite occurs as thin ribbon-like crystals, up to 5 mm in length but only a few μm in thickness, sometimes bent to form curls and rings (Figure 1). Ribbon-like crystals are formed by the parallel association of several individuals. Thallium-bearing chovanite is associated with (Tl,Ag)-bearing rouxelite, robinsonite, sphalerite, valentinite, baryte, dolomite, quartz, and "hyalophane" (Ba-rich K-feldspar), in vugs of dolomite ± baryte ± quartz veins embedded in the metadolostone of the Sant'Olga level, Monte Arsiccio mine, Apuan Alps.

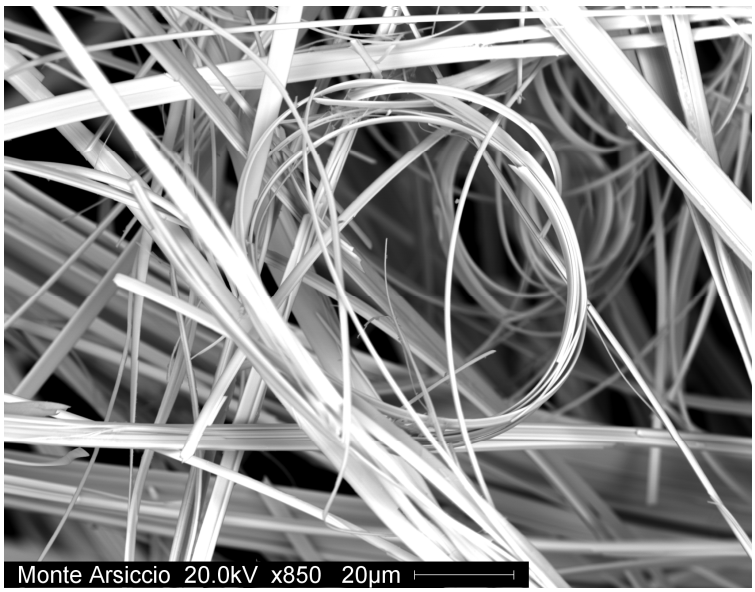


**Figure 1.** Chovanite, ribbon-like crystals and curls. Sant'Olga level, Monte Arsiccio mine, Apuan Alps, Tuscany, Italy.

Chemical data, reported in [2], corresponded to the following chemical formulae, recalculated on the basis of Σ*Me* = 58 apfu: $Ag_{0.30}Tl_{0.72}Pb_{25.75}Sb_{29.42}As_{1.84}S_{71.18}Cl_{0.06}$ and $Ag_{0.30}Tl_{0.86}Pb_{25.56}Sb_{29.59}As_{1.69}S_{71.52}Se_{0.07}Cl_{0.05}$. Subtracting Ag, Se, and Cl, according to the substitution rules $Ag^{+} + Sb^{3+} = 2Pb^{2+}$, $Se^{2-} = S^{2-}$, and $Pb^{2+} + Cl^{-} = Sb^{3+} + S^{2-}$, the two formulae become $Tl_{0.72}Pb_{26.29}(Sb_{29.18}As_{1.84})_{\Sigma=31.02}S_{71.24}$ and $Tl_{0.86}Pb_{25.81}(Sb_{29.34}As_{1.69})_{\Sigma=31.03}S_{71.64}$, respectively. Assuming the occurrence of 1 O apfu, as suggested by the crystal structure study [2], they correspond to the ideal formula $TlPb_{26}(Sb,As)_{31}S_{72}O$.

## 3. Crystallography

For the X-ray single-crystal diffraction study, the intensity data were collected at the XRD1 beamline, ELETTRA synchrotron facility [3]. A monochromatic wavelength of 0.59040 Å (21.00 k*e*V) has been used on a 50 × 50 $\mu m^2$ beam size, using a Dectris Pilatus 2M hybrid pixel area detector, at a

sample-detector distance of 85 mm. The diffraction data, collected at room temperature, were indexed, integrated, and scaled using the XDS software package [4]. The data were corrected for the Lorentz and polarization factors using XDS [4] built-in algorithms.

Tests on the distribution of $|E|$ values agree with the occurrence of an inversion center ($|E^2 - 1| = 0.879$). This information, together with systematic absences, agrees with the space group, $P2_1/c$. The refined unit-cell parameters are $a$ = 34.280(3), $b$ = 8.2430(7), $c$ = 48.457(4) Å, β = 106.290(4)°, $V$ = 13143(2) Å$^3$, and $Z$ = 4.

The crystal structure was refined with *Shelxl*-2018 [5] starting from the atomic coordinates of chovanite [2]. The site occupancy factors (s.o.f.) were refined using the scattering curves for neutral atoms given in the *International Tables for Crystallography* [6]. Several mixed Pb/Sb and Sb/As positions were found, whereas *Me*13 and *Me*14 sites (labeled Pb13 and Pb14 in [2]) were found to be split. Their s.o.f. were refined using the scattering curves of Pb and Tl at the *Me*13a/*Me*14a and *Me*13b/*Me*14b positions, respectively. After several cycles of anisotropic refinement, a final $R_1$ = 0.0826 for 12,052 reflections with $F_o > 4\sigma(F_o)$ and 1210 refined parameters was obtained. Crystal data and details of the intensity data collection and refinement are reported in Table 1.

**Table 1.** Crystal and experimental details for thallium-bearing chovanite.

| **Crystal Data** | |
|---|---|
| Crystal size (mm$^3$) | 0.080 × 0.010 × 0.010 |
| Cell setting, space group | Monoclinic, $P2_1/c$ |
| $a$ (Å) | 34.280(3) |
| $b$ (Å) | 8.2430(7) |
| $c$ (Å) | 48.457(4) |
| β (°) | 106.290(4) |
| $V$ (Å$^3$) | 13143(2) |
| $Z$ | 4 |
| **Data Collection and Refinement** | |
| Radiation, wavelength (Å) | synchrotron, λ = 0.59040 |
| Temperature (K) | 293 |
| $2\theta_{max}$ (°) | 45.71 |
| Measured reflections | 96,021 |
| Unique reflections | 31,011 |
| Reflections with $F_o > 4\sigma(F_o)$ | 12,052 |
| $R_{int}$ | 0.1732 |
| $R\sigma$ | 0.1696 |
| Range of $h$, $k$, $l$ | $-45 \leq h \leq 44$, $-10 \leq k \leq 10$, $-63 \leq l \leq 63$ |
| $R_1$ [$F_o > 4\sigma(F_o)$] | 0.0826 |
| $R_1$ (all data) | 0.2065 |
| $wR_2$ (on $F_o^2$) | 0.2408 |
| GooF | 0.946 |
| Number of least-squares parameters | 1210 |
| Maximum and minimum residual peak ($e$ Å$^{-3}$) | 3.15 (at 0.75 Å from Pb9)<br>−3.77 (at 0.58 Å from Pb40) |

Atomic coordinates, site occupancies, and displacement parameters are available in the Crystallographic Information File, available as a Supplementary Material. Table 2 gives site occupation factors (s.o.f.), average <*Me*–Φ> distances (Φ = S, O), and bond-valence sums for cation positions only. Bond-valence sums (BVS) for anions are given in Table 3. Bond parameters for Pb–S, Sb–S, and As–S bonds are taken from [7], whereas the value of 2.55 Å proposed by [8] for the pair Tl–S was used. Finally, the bond-valence sum for oxygen was calculated using the bond parameters given by Brese and O'Keeffe [7], Mills et al. [9], and Krivovichev [10] for $As^{3+}$–O, $Sb^{3+}$–O, and $Pb^{2+}$–O, respectively.

**Table 2.** Site occupancy factors (s.o.f.), average <*Me*–Φ> (Φ = S, O) distances (in Å), and bond-valence sums (BVS) in valence units (v.u.) for cation positions.

| Site | s.o.f. | <*Me*–Φ> | BVS | Site | s.o.f. | <*Me*–Φ> | BVS |
|---|---|---|---|---|---|---|---|
| Pb1 | $Pb_{1.00}$ | 3.098 | 1.87 | Sb29 | $Sb_{0.92(3)}As_{0.08(3)}$ | 2.439 | 3.17 |
| Pb2 | $Pb_{1.00}$ | 3.106 | 1.82 | Sb30 | $Sb_{1.00}$ | 2.740 | 2.61 |
| Pb3 | $Pb_{1.00}$ | 3.106 | 1.81 | Sb31 | $Sb_{1.00}$ | 2.529 | 2.79 |
| Pb4 | $Pb_{1.00}$ | 3.103 | 1.84 | Sb32 | $Sb_{1.00}$ | 2.461 | 3.08 |
| Pb5 | $Pb_{1.00}$ | 3.090 | 1.88 | Pb33 | $Pb_{1.00}$ | 3.052 | 1.91 |
| Pb6 | $Pb_{1.00}$ | 3.090 | 1.87 | Pb34 | $Pb_{1.00}$ | 3.039 | 1.95 |
| Pb7 | $Pb_{1.00}$ | 3.136 | 1.89 | Pb35 | $Pb_{0.72(1)}Sb_{0.28(1)}$ | 3.069 | 2.10 |
| Pb8 | $Pb_{1.00}$ | 3.130 | 1.97 | Pb36 | $Pb_{1.00}$ | 3.110 | 1.87 |
| Pb9 | $Pb_{1.00}$ | 3.142 | 1.84 | Pb37 | $Pb_{1.00}$ | 3.135 | 1.75 |
| Pb10 | $Pb_{1.00}$ | 3.130 | 1.86 | Sb38 | $Sb_{0.95(1)}Pb_{0.05(1)}$ | 3.017 | 2.69 |
| Sb11 | $Sb_{0.63(2)}Pb_{0.37(2)}$ | 3.042 | 2.31 | Sb39 | $Sb_{1.00}$ | 2.490 | 2.89 |
| Sb12 | $Sb_{0.61(2)}Pb_{0.39(2)}$ | 3.050 | 2.13 | Pb40 | $Pb_{1.00}$ | 3.126 | 2.12 |
| *Me*13a | $Pb_{0.65(1)}$ | 3.237 | 1.02 | Sb41 | $Sb_{0.94(1)}Pb_{0.06(1)}$ | 3.032 | 2.89 |
| *Me*13b | $Tl_{0.35(1)}$ | 3.284 | 0.44 | Pb42 | $Pb_{1.00}$ | 3.073 | 2.03 |
| *Me*14a | $Pb_{0.80(3)}$ | 3.248 | 1.33 | Pb43 | $Pb_{1.00}$ | 3.097 | 2.19 |
| *Me*14b | $Tl_{0.20(3)}$ | 3.229 | 0.30 | Pb44 | $Pb_{0.90(1)}Sb_{0.10(1)}$ | 3.028 | 2.09 |
| Sb15 | $Sb_{0.93(3)}As_{0.07(3)}$ | 2.554 | 2.81 | Sb45 | $Sb_{0.86(3)}As_{0.14(3)}$ | 2.287 | 2.99 |
| As16 | $As_{0.59(3)}Sb_{0.41(3)}$ | 2.341 | 3.28 | Sb46 | $Sb_{1.00}$ | 2.376 | 2.89 |
| Sb17 | $Sb_{0.87(3)}As_{0.13(3)}$ | 2.471 | 2.99 | Sb47 | $Sb_{0.94(1)}Pb_{0.06(1)}$ | 2.961 | 2.65 |
| Sb18 | $Sb_{1.00}$ | 2.529 | 2.91 | Sb48 | $Sb_{1.00}$ | 2.472 | 3.05 |
| Pb19 | $Pb_{1.00}$ | 3.027 | 2.00 | Sb49 | $Sb_{0.92(2)}Pb_{0.08(2)}$ | 2.958 | 2.59 |
| Pb20 | $Pb_{1.00}$ | 3.024 | 2.12 | Sb50 | $Sb_{1.00}$ | 2.540 | 2.81 |
| Sb21 | $Sb_{1.00}$ | 2.516 | 2.90 | Sb51 | $Sb_{1.00}$ | 2.920 | 2.66 |
| Sb22 | $Sb_{1.00}$ | 2.474 | 3.04 | Sb52 | $Sb_{0.70(2)}Pb_{0.30(2)}$ | 3.062 | 2.18 |
| Sb23 | $Sb_{1.00}$ | 2.500 | 2.92 | Sb53 | $Sb_{1.00}$ | 2.514 | 2.89 |
| Sb24 | $Sb_{1.00}$ | 2.559 | 2.79 | Sb54 | $Sb_{1.00}$ | 2.509 | 2.85 |
| Sb25 | $Sb_{0.94(3)}As_{0.06(3)}$ | 2.502 | 2.88 | Sb55 | $Sb_{0.57(3)}As_{0.43(3)}$ | 2.386 | 3.23 |
| Sb26 | $Sb_{0.92(2)}Pb_{0.08(2)}$ | 2.926 | 2.57 | Sb56 | $Sb_{0.96(1)}Pb_{0.04(1)}$ | 2.762 | 2.60 |
| Pb27 | $Pb_{1.00}$ | 3.024 | 2.00 | Sb57 | $Sb_{1.00}$ | 2.528 | 2.94 |
| Pb28 | $Pb_{1.00}$ | 3.023 | 2.06 | Sb58 | $Sb_{1.00}$ | 2.569 | 2.75 |

**Table 3.** Bond-valence sums (BVS) in valence units (v.u.) for anion positions.

| Site | BVS | Site | BVS | Site | BVS | Site | BVS |
|---|---|---|---|---|---|---|---|
| S1 | 1.97 | S19 | 1.86 | S37 | 1.72 | S55 | 1.81 |
| S2 | 1.94 | S20 | 1.94 | S38 | 1.74 | S56 | 1.86 |
| S3 | 1.90 | S21 | 2.14 | S39 | 1.74 | S57 | 1.78 |
| S4 | 1.98 | S22 | 2.13 | S40 | 1.76 | S58 | 1.85 |
| S5 | 1.96 | S23 | 1.80 | S41 | 2.04 | S59 | 1.96 |
| S6 | 1.94 | S24 | 1.85 | S42 | 2.04 | S60 | 1.89 |
| S7 | 2.06 | S25 | 1.76 | S43 | 2.06 | S61 | 1.81 |
| S8 | 2.00 | S26 | 1.88 | S44 | 2.09 | S62 | 1.88 |
| S9 | 1.99 | S27 | 1.85 | S45 | 2.03 | S63 | 2.15 |
| S10 | 2.03 | S28 | 1.77 | S46 | 1.77 | S64 | 2.02 |
| S11 | 1.98 | S29 | 1.82 | S47 | 1.80 | S65 | 1.91 |
| S12a/S12b * | 0.81/0.81 | S30 | 1.81 | S48 | 1.98 | S66 | 1.74 |
| S13 | 2.02 | S31 | 2.21 | S49 | 1.72 | S67 | 1.59 |
| S14 | 1.97 | S32 | 2.05 | S50 | 1.73 | S68 | 1.74 |
| S15 | 2.03 | S33 | 2.14 | S51 | 2.16 | S69 | 2.00 |
| S16 | 2.12 | S34 | 2.12 | S52 | 2.04 | S70 | 2.26 |
| S17 | 1.89 | S35 | 1.82 | S53 | 2.15 | S71 | 1.78 |
| S18 | 1.81 | S36 | 1.79 | S54 | 2.13 | S72 | 1.97 |
| O | 1.99 | | | | | | |

* Weighted according to refined s.o.f.

## 4. X-ray Absorption Spectroscopy

X-ray Absorption Spectroscopy (XAS) measurements at the Tl-$L_3$ edge (12,658 *e*V) were performed at ~20 K on beamline ID26 at the European Synchrotron Radiation Facility (ESRF). The spectrum was measured in high-energy resolution fluorescence-detected (HERFD). The Tl $L\alpha_1$ emission line (10,269 *e*V) was selected using the 555 reflection of five spherically bent (radius = 0.5 m) Si analyzer crystals (diameter = 100 mm) in a vertical Rowland geometry [11]. Diffracted intensity was collected using a Silicon Drift Detector (SDD); the effective energy resolution was ~3.0 *e*V. The incoming beam was monochromatized using the 111 reflection of a Si double crystal monochromator, focused on the sample via two Pd-coated Si mirrors in the Kirkpatrick–Baez configuration.

The X-ray Absorption Near Edge Structure (XANES) spectrum (normalized and first derivative) of chovanite is reported in Figure 2. The peak in the derivative indicates the position of the main inflection point, which, by convention, is considered to be the absorption edge energy. The XANES region shows the typical characteristics of monovalent Tl, having a single absorption peak with an absorption edge at ~12,663 *e*V ([12] and references therein).

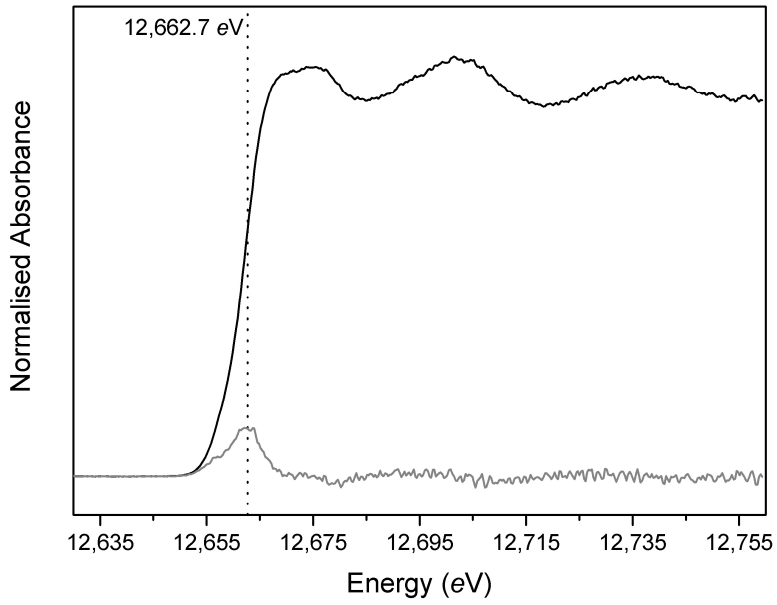


**Figure 2.** Normalized (black) and first derivative (grey) Tl $L_3$-edge X-ray Absorption Near Edge Structure (XANES) spectrum.

## 5. Results and Discussion

### *5.1. Crystal Structure Description*

The crystal structure of thallium-rich chovanite, shown in Figure 3, agrees with [2]. Among the 58 cation positions occurring in its crystal structure, there are 21 pure Pb sites, two mixed and split Pb/Tl positions, 11 mixed Pb/Sb sites, 17 pure Sb positions, and 7 mixed Sb/As sites. The geometrical features of these sites agree with those described in [2]. Similarly, among the seventy-two S positions, S12 is split into two sub-sites, with a ratio between S12a and S12b of 0.65/0.35.

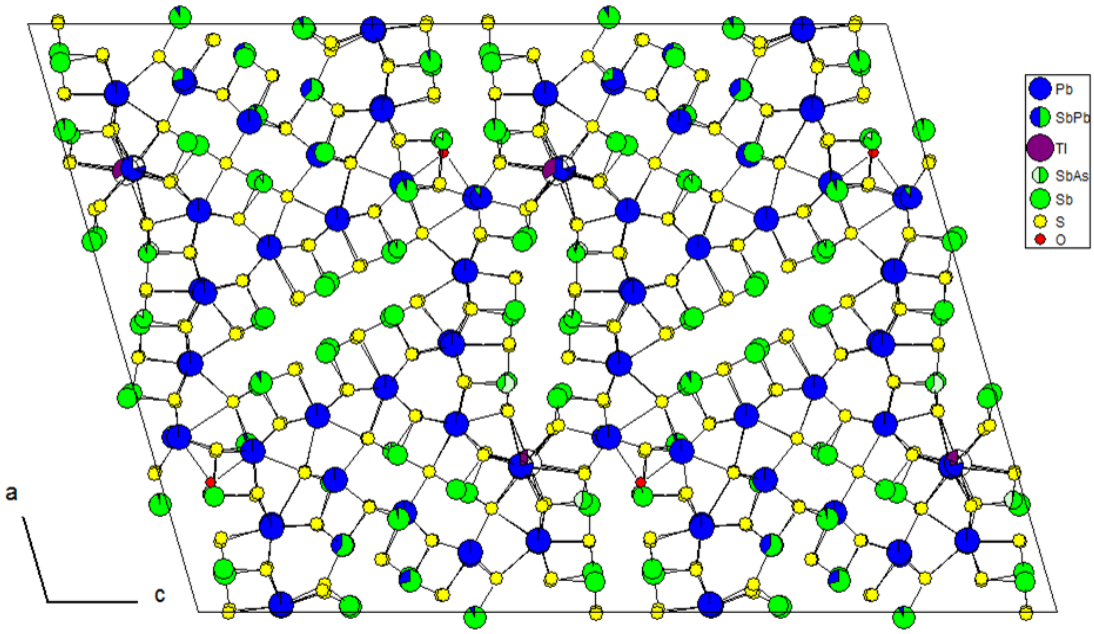


**Figure 3.** Unit-cell content of Tl-bearing chovanite as viewed down the **b**-axis.

The crystal structure of chovanite has been detailed on the basis of a sample from the Pollone mine, according to the general approach developed by [13] for sulfosalts with rod-based structures related to SnS or PbS archetypes. Chovanite belongs to the group of sulfosalts having a boxwork architecture [14]. Its crystal structure can be obtained by combining three distinct kinds of modules, i.e., walls, partitions, and fill elements, labeled as C (i.e., C1 + C2), A, and B in Figure 4. Table 4 compares the chemical composition of these modules between the Monte Arsiccio and Pollone samples.

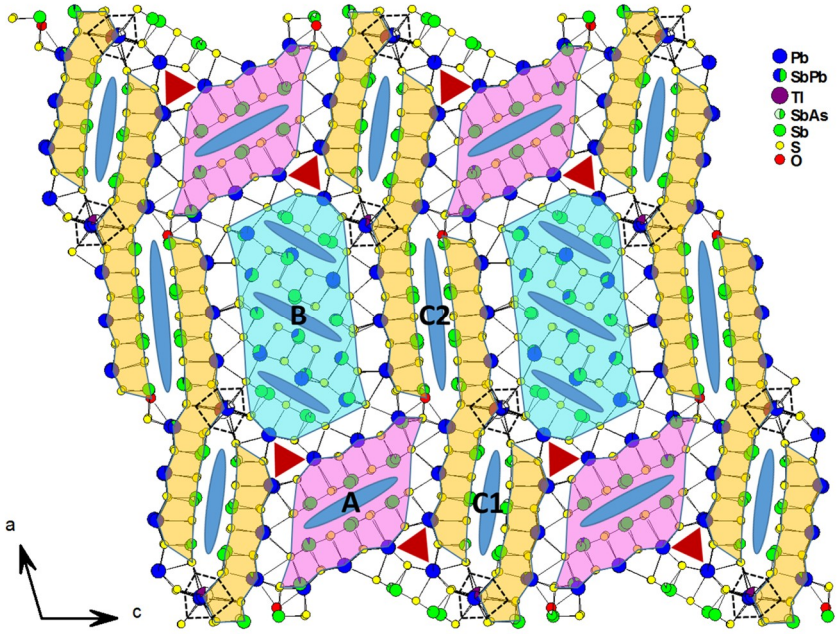


**Figure 4.** Projection along the **b**-axis of the crystal structure of Tl-bearing chovanite. The different kinds of modules are shown: A = pink; B = light blue; and C (i.e., C1 + C2) = yellow.

**Table 4.** Comparison of module compositions between crystal structures of chovanite from Monte Arsiccio (MA—this study) and Pollone (P—[2]).

| Module | | Formula | As/(Sb + As) | Pb/Σ*Me* |
|---|---|---|---|---|
| Rod A (partition) | MA | $Pb_5(Sb_{1.86}Pb_{0.14})_{\Sigma=2}Sb_4(Sb_{0.94}As_{0.06})_{\Sigma=1}S_{16}$ | 0.009 | 0.428 |
| (=$Me_{12}S_{16}$) | P | $Pb_5(Sb_{1.55}Pb_{0.45})_{\Sigma=2}Sb_4(Sb_{0.91}As_{0.09})_{\Sigma=1}S_{16}$ | 0.014 | 0.454 |
| Rod B (fill element) | MA | $Pb_5(Sb_{4.09}Pb_{1.91})_{\Sigma=6}Sb_6(Sb_{0.92}As_{0.08})_{\Sigma=1}S_{26}$ | 0.007 | 0.384 |
| (=$Me_{18}S_{26}$) | P | $Pb_5(Sb_{2.58}Pb_{2.42})_{\Sigma=5}Sb_3(Sb_{3.94}As_{1.06})_{\Sigma=5}S_{26}$ | 0.100 | 0.412 |
| Rod-layer C (wall) | | | | |
| C1 Rod | MA | $Pb_5(Sb_{0.10}Pb_{0.90})_{\Sigma=1}Sb_3(Sb_{2.21}As_{0.79})_{\Sigma=3}S_{14}$ | 0.130 | 0.492 |
| (=$Me_{12}S_{14}$) | P | $Pb_6Sb_3(Sb_{1.49}As_{0.51})_{\Sigma=2}AsS_{14}$ | 0.252 | 0.500 |
| C2 Rod | MA | $(Pb_{1.45}Tl_{0.55})_{\Sigma=2}Pb_6(Sb_{1.90}Pb_{0.10})_{\Sigma=2}Sb_4(Sb_{1.44}As_{0.56})_{\Sigma=2}S_{16}O$ | 0.071 | 0.472 |
| (=$Me_{16}S_{16}O$) | P | $Pb_8(Sb_{1.58}Pb_{0.42})_{\Sigma=2}Sb_3(Sb_{1.19}As_{0.81})_{\Sigma=2}AsS_{16}O$ | 0.239 | 0.526 |
| Sum | MA | $(Pb_{1.45}Tl_{0.55})_{\Sigma=2}Pb_{21}(Sb_{7.95}Pb_{3.05})_{\Sigma=11}Sb_{17}(Sb_{5.51}As_{1.49})_{\Sigma=7}S_{72}O$ | 0.047 | 0.440 |
| (=$Me_{58}S_{72}O$) | P | $Pb_{24}(Sb_{5.71}Pb_{3.29})_{\Sigma=9}Sb_{13}(Sb_{7.53}As_{2.47})_{\Sigma=10}As_2S_{72}O$ | 0.146 | 0.471 |

The simplified formula of the Monte Arsiccio crystal structure is $Tl_{0.55}Pb_{25.50}(Sb_{30.46}As_{1.49})_{\Sigma=31.95}S_{72}O$, which has a positive valence balance *Ev*% = +1.0 [*Ev*(%) = [Σval(+) − Σval(−)] × 100/Σval(−)], related to an overestimation of Sb with respect to Pb. This may be due to the occurrence of minor Ag. Owing to the similar scattering factors of Ag (*Z* = 47) and Sb (*Z* = 51), minor Ag (0.30 apfu) is difficult to locate in the crystal structure of chovanite. On the basis of BVS values, Ag could be placed at some undersaturated Sb or mixed (Sb/Pb) positions. For instance, Sb52 has a BVS value significantly lower than that expected on the basis of the s.o.f., i.e., 2.18 v.u. vs. 2.70 v.u. This could be related to the occurrence of Ag, with an s.o.f. ($Ag_{0.35}Sb_{0.35}Pb_{0.30}$), resulting in an expected BVS of 2 v.u. Moreover, Tl is underestimated with respect to chemical analyses (Tl ranging between 0.72 and 0.86 apfu). However, its actual content could be estimated only on the basis of the bond-valence approach (see below).

Arsenic is virtually absent in rods A and B (only 0.06 and 0.08 apfu, respectively), whereas it is concentrated in rod-layers C, see Table 4. Arsenic occurs in six mixed (Sb/As) sites and it is dominant over Sb only in one of them (As16). In every module, see Table 4, the As/(Sb + As) atomic ratio of chovanite from the Pollone mine is over that of the sample from Monte Arsiccio. The As partitioning is not related to the Pb/Σ*Me* ratio.

The solution of the crystal structure agrees with the occurrence of one O atom per formula unit, with oxygen alternating with a vacancy along the **b**-axis, as shown in Figure 5. Oxygen is bonded to a pure Sb site (Sb46) and a mixed (Sb,As) site (Sb45), with (Sb/As)–O distances of 2.01(2) and 1.97(2) Å, respectively. The Sb45–O–Sb46 angle is 138(1)°. These distances are slightly longer than those observed in chovanite from the Pollone mine [2], where As was the dominant cation at the Sb45 position. This kind of configuration is topologically identical to those observed for the O3 isolated oxygen in scainiite [15], in a synthetic (Pb,Mn,Sb) oxy-chloro-sulfide [16], in pillaite [17], pellouxite [18], and meerschautite [19].

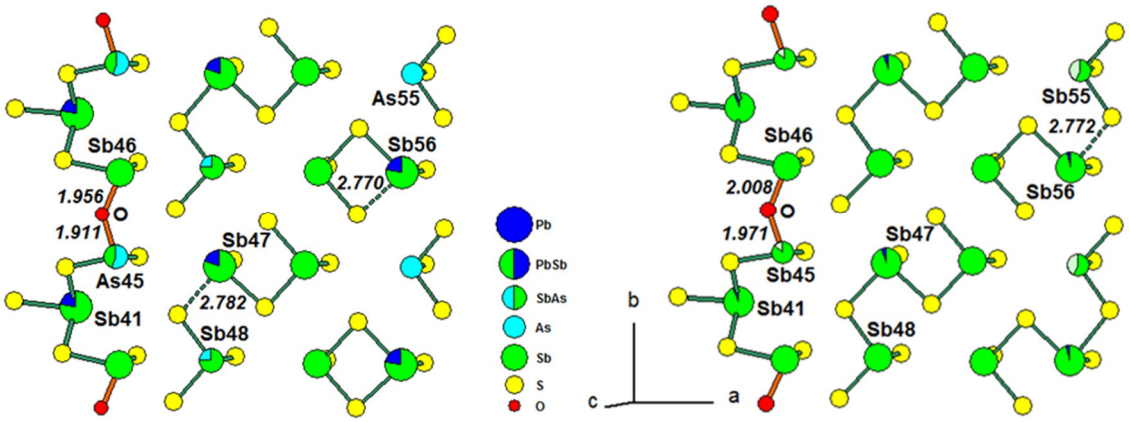


**Figure 5.** (Sb,As)–S polymerization in C2 rods from Pollone (**left**) and Monte Arsiccio (**right**).

In chovanite from Pollone [2], the selection of the shortest (=strongest) (Sb,As)–S bonds ($\leq$2.70 Å), together with short (Sb,As)–O distances distinguish finite $(Sb,As)_mS_n$ chain fragments within the four constitutive modules A, B, C1, and C2. These chain fragments also contain mixed (Sb,Pb) positions. When Pb is present on these positions, it breaks the chains into shorter $(Sb,As)_mS_n$ groups.

In chovanite from Monte Arsiccio, the chain topology is identical to that described in chovanite from Pollone in rods A and C1, as well as in the lateral ribbon of rod B. In the central ribbon of rod B, the variety of mixed (Sb,Pb) sites excludes a simple chain description. In rod C2, there are only two finite groups, compared to three at Pollone, see Figure 5:

Monte Arsiccio: $[Sb(Sb_{0.94}Pb_{0.06})SbS_7]\cdot[Sb(Sb_{0.94}Pb_{0.06})(Sb_{0.57}As_{0.43})S_7]$.

Pollone: $[(Sb_{0.75}As_{0.25})(Sb_{0.80}Pb_{0.20})SbS_7]\cdot[Sb(Sb_{0.78}Pb_{0.22})S_4]\cdot[AsS_3]$.

This is due to the higher Sb content on (Sb,Pb) positions (Sb47 and Sb56) as well as on mixed (Sb,As) (Sb55).

### *5.2. Thallium in the Crystal Structure of Chovanite*

Chovanite from the Slovak locality is Tl-free [1], whereas the chovanite from the Pollone mine has 0.30 Tl apfu [2]. According to [2], in the 8 Å crystal structure of chovanite, the sites Pb13 and Pb14 have the highest coordination number (IX) and were considered as the most favorable to host the large cation $Tl^+$. In the crystal structure of chovanite from the Pollone mine, thallium was likely hosted at the split Pb13b position (labeled *Me*13b in the sample from Monte Arsiccio), although minor amounts of this element should also be disordered at the Pb13a and Pb14 sites (i.e., *Me*13a and *Me*14).

The higher Tl content of chovanite from the Monte Arsiccio Mine allows a better understanding of the partitioning of this element. Owing to the similar scattering factors of Tl ($Z$ = 81) and Pb ($Z$ = 82), the only way to propose a distribution of these two elements, using conventional X-ray diffraction, is taking into account the bond-valence sums. In agreement with [8], we used a value of $R_{Tl,S}$ = 2.55 Å, instead of the value of 2.63 Å given by [7].

In Tl-bearing chovanite, both *Me*13 and *Me*14 sites were found to be split. Assuming the full-occupancy of these positions, the following BVS can be calculated (in v.u.): 1.57 (*Me*13a), 1.27 (*Me*13b), 1.68 (*Me*14a), and 1.51 (*Me*14b). The average <*Me*–S> distances range between 3.229 (*Me*14b) and 3.285 Å (*Me*13b). Taking into account BVS values and the refined site scatterings (refined assuming Pb at the *Me*13a and *Me*14a sites and Tl at the *Me*13b and *Me*14b sites—see Table 2), the following site populations at the four sub-sites could be proposed: $Pb_{0.42}Tl_{0.23}$ at *Me*13a, $Tl_{0.26}Pb_{0.09}$ at *Me*13b, $Pb_{0.55}Tl_{0.25}$ at *Me*14a, and $Pb_{0.10}Tl_{0.10}$ at *Me*14b. Consequently, the site populations at *Me*13 and *Me*14 are $Pb_{0.51}Tl_{0.49}$ and $Pb_{0.65}Tl_{0.35}$, respectively, with a total Tl content of 0.84 apfu, in agreement with the chemical data. Taking into account such a population, the structural formula of Tl-bearing chovanite could be written as $Tl_{0.84}Pb_{25.21}(Sb_{30.46}As_{1.49})_{\Sigma=31.95}S_{72}O$ ($Ev$% = +0.8).

Monovalent Tl substituting divalent Pb induces a deficit of positive charges. Relatively to Pollone chovanite, this is partly compensated by a Sb increase in two neighbouring sites: $(Sb_{0.96}Pb_{0.04})$ against $(Sb_{0.78}Pb_{0.22})$ at Sb56 and $(Pb_{0.90}Sb_{0.10})$ against pure Pb at Pb44.

## 6. Conclusions

The crystal-chemical characterization of Tl-bearing chovanite from Monte Arsiccio allowed the distribution of monovalent Tl between two positions, with a preferential partitioning at the *Me*13 site, to be described. However, Pb is still dominant in both sites, and the studied samples should be considered as a Tl-rich variety of chovanite. Likely, the crystallization of chovanite in hydrothermal environments richer in Tl than that responsible for the formation of the Monte Arsiccio ore assemblage could favor the existence of the Tl-analogue of chovanite, with Tl dominant over Pb at the *Me*13 position.

Thallium-bearing chovanite is the third Pb-Sb sulfosalt from the Monte Arsiccio mine showing the presence of a minor amount of Tl in its crystal structure, after rouxelite [20] and andreadiniite [21], thus reflecting the complex ore geochemistry of this ore deposit, where minor components (Ag, Cu, Hg, Tl),

peculiar $f(O_2)/f(S_2)$ conditions, and subtle variations in the Pb/(Sb,As) atomic ratios promoted the crystallization of a wide variety of sulfosalt species.

**Supplementary Materials:** The following are available online at http://www.mdpi.com/2075-163X/8/11/535/s1, CIF: Tl-bearing chovanite.

**Author Contributions:** C.B. conceived and designed the experiments; N.P., N.D., and G.O.L. performed the experiments; C.B. and Y.M. analyzed the chemical and crystallographic data; G.O.L. analyzed the XAS data; C.B. and Y.M. wrote the paper with input from N.P., N.D., and G.O.L.

**Acknowledgments:** This research was supported by MIUR through the project SIR 2014 "THALMIGEN–Thallium: Mineralogy, Geochemistry, and Environmental Hazards" granted to CB (Grant No. RBSI14A1CV) and by the University of Pisa through the project P.R.A. 2018-2019 "Georisorse e Ambiente" (Grant No. PRA_2018_41). Alain Manceau is thanked for the use of the 0.5 m Si analyzer crystals [financial support from the ANR grant ANR-10-EQPX-27-01 (EcoX Equipex) to Alain Manceau and Pieter Glatzel]. Blanka Detlefs and Tim Bohdan are thanked for the assistance during measurements on ID26 beamline.

**Conflicts of Interest:** The authors declare no conflict of interest.

## References

1. Topa, D.; Sejkora, J.; Makovicky, E.; Pršek, J.; Ozdín, D.; Putz, H.; Dittrich, H.; Karup-Møller, S. Chovanite, $Pb_{15-2x}Sb_{14+2x}S_{36}O_x$ (x~0.2), a new sulphosalt species from the Low Tatra Mountains, Western Carpathians, Slovakia. *Eur. J. Mineral.* **2012**, *24*, 727–740. [CrossRef]
2. Biagioni, C.; Moëlo, Y. Lead-antimony sulfosalts from Tuscany (Italy). XIX. Crystal chemistry of chovanite from two new occurrences in the Apuan Alps and its 8 Å crystal structure. *Mineral. Mag.* **2017**, *81*, 811–831. [CrossRef]
3. Lausi, A.; Polentarutti, M.; Onesti, S.; Plaisier, J.R.; Busetto, E.; Bais, G.; Barba, L.; Cassetta, A.; Campi, G.; Lamba, D.; et al. Status of the crystallography beamlines at Elettra. *Eur. Phys. J. Plus* **2015**, *130*, 43–51. [CrossRef]
4. Kabsch, W. Integration, scaling, space-group assignment and post-refinement. *Acta Crystallogr.* **2010**, *D66*, 125–132. [CrossRef] [PubMed]
5. Sheldrick, G.M. Crystal structure refinement with SHELXL. *Acta Crystallogr.* **2015**, *C71*, 3–8.
6. Wilson, A.J.C. (Ed.) *International Tables for Crystallography. Volume C: Mathematical, Physical and Chemical Tables*; Kluwer Academic: Dordrecth, The Netherlands, 1992.
7. Brese, N.E.; O'Keeffe, M. Bond-valence parameters for solids. *Acta Crystallogr.* **1991**, *B47*, 192–197. [CrossRef]
8. Biagioni, C.; Bonaccorsi, E.; Moëlo, Y.; Orlandi, P.; Bindi, L.; D'Orazio, M.; Vezzoni, S. Mercury-arsenic sulfosalts from the Apuan Alps (Tuscany, Italy). II. Arsiccioite, $AgHg_2TlAs_2S_6$, a new mineral from the Monte Arsiccio mine: Occurrence, crystal structure and crystal chemistry of the routhierite isotypic series. *Mineral. Mag.* **2014**, *78*, 101–117. [CrossRef]
9. Mills, S.J.; Christy, A.G.; Chen, E.C.-C.; Raudsepp, M. Revised values of the bond valence parameters for $^{[6]}$Sb(V)–O and $^{[3-11]}$Sb(III)–O. *Z. Krist.* **2009**, *224*, 423–431. [CrossRef]
10. Krivovichev, S.V. Derivation of bond-valence parameters for some cation-oxygen pairs on the basis of empirical relationships between $r_0$ and *b*. *Z. Krist.* **2012**, *227*, 575–579.
11. Rovezzi, M.; Lapras, C.; Manceau, A.; Glatzel, P.; Verbeni, R. High energy-resolution X-ray spectroscopy at ultra-high dilution with spherically bent crystal analyzers of 0.5 m radius. *Rev. Sci. Instrum.* **2017**, *88*, 013108. [CrossRef] [PubMed]
12. Biagioni, C.; D'Orazio, M.; Lepore, G.O.; d'Acapito, F.; Vezzoni, S. Thallium-rich rust scales in drinkable water distribution systems: A case study from northern Tuscany, Italy. *Sci. Total Environ.* **2017**, *587*, 491–501. [CrossRef] [PubMed]
13. Makovicky, E. Rod-based sulphosalt structures derived from the SnS and PbS archetype. *Eur. J. Mineral.* **1993**, *5*, 545–591. [CrossRef]
14. Makovicky, E.; Topa, D. The crystal structure of sulfosalts with the boxwork architecture and their new representative, $Pb_{15-2x}Sb_{14+2x}S_{36}O_x$. *Can. Mineral.* **2009**, *47*, 3–24. [CrossRef]
15. Moëlo, Y.; Meerschaut, A.; Orlandi, P.; Palvadeau, P. Lead-antimony sulfosalts from Tuscany (Italy). II. Crystal structure of scainiite, $Pb_{14}Sb_{30}S_{54}O_5$, an expanded monoclinic derivative of $Ba_{12}Bi_{24}S_{48}$ hexagonal sub-type (zinkenite group). *Eur. J. Mineral.* **2000**, *12*, 835–846. [CrossRef]

16. Doussier, C.; Moëlo, Y.; Léone, P.; Meerschaut, A. $(Mn_{1-x}Pb_x)Pb_{10+y}Sb_{12-y}S_{26-y}Cl_{4+y}O$, a new oxy-chloro-sulfide with ~2 nm-spaced $(Mn,Pb)Cl_4$ single chains within a waffle-type crystal-structure. *J. Solid State Chem.* **2007**, *180*, 2323–2334. [CrossRef]
17. Meerschaut, A.; Palvadeau, P.; Moëlo, Y.; Orlandi, P. Lead-antimony sulfosalts from Tuscany (Italy). IV. Crystal structure of pillaite, $Pb_9Sb_{10}S_{23}ClO_{0.5}$, an expanded monoclinic derivative of hexagonal $Bi(Bi_2S_3)_9I_3$, from the zinkenite group. *Eur. J. Mineral.* **2001**, *13*, 779–790. [CrossRef]
18. Palvadeau, P.; Meerschaut, A.; Orlandi, P.; Moëlo, Y. Lead-antimony sulfosalts from Tuscany (Italy). VII. Crystal structure of pellouxite, $\sim(Cu,Ag)_2Pb_{21}Sb_{23}S_{55}ClO$, an expanded monoclinic derivative of $Ba_{12}Bi_{24}S_{48}$ hexagonal sub-type (zinkenite group). *Eur. J. Mineral.* **2004**, *16*, 845–855. [CrossRef]
19. Biagioni, C.; Moëlo, Y.; Orlandi, P.; Stanley, C.J. Lead-antimony sulfosalts from Tuscany (Italy). XVII. Meerschautite, $(Ag,Cu)_{5.5}Pb_{42.4}(Sb,As)_{45.1}S_{112}O_{0.8}$, a new expanded derivative of owyheeite from the Pollone mine, Valdicastello Carducci: occurrence and crystal structure. *Mineral. Mag.* **2016**, *80*, 675–690. [CrossRef]
20. Biagioni, C.; Moëlo, Y.; Orlandi, P. Lead-antimony sulfosalts from Tuscany (Italy). XV. (Tl-Ag)-bearing rouxelite from Monte Arsiccio mine: Occurrence and crystal chemistry. *Mineral. Mag.* **2014**, *78*, 651–661. [CrossRef]
21. Biagioni, C.; Moëlo, Y.; Orlandi, P.; Paar, W.H. Lead-antimony sulfosalts from Tuscany (Italy). XXIII. Andreadiniite, $CuAg_7HgPb_7Sb_{24}S_{48}$, a new oversubstituted (Cu,Hg)-rich member of the andorite homeotypic series from the Monte Arsiccio mine, Apuan Alps. *Eur. J. Mineral.* **2018**, *30*, 1021–1035. [CrossRef]